

# Efficient technique for lucky frame selection using phase diversity images.

S. Woods, J. G. Burnett, A. M. Scott  
QinetiQ Ltd., St Andrews Road  
Great Malvern, WR14 3PS

## Abstract

*Lucky sub-frame selection can be used to improve the quality of imagery degraded by anisoplanatic atmospheric turbulence. The technique works by recording multiple images of the scene, identifying regions in each frame that are of high quality, and compiling these “lucky sub-frames” into a composite high quality image. To operate in real-time, the technique requires a rapid method of assessing the varying image quality across the field-of-view. This paper describes an initial study into the use of low-resolution phase-diverse images to provide this quality information. The method offers a significant speed improvement over the standard image sharpness calculation (by a factor of 13 in the proof-of-concept model). The results showed an improvement of a factor of 2-2.5 in the modulation transfer function at high spatial frequencies.*

Keywords: Lucky imaging, Speckle imaging, Phase-diversity, Wavefront sensor

## Introduction

Long range imaging at low altitude is subject to image degradation due to atmospheric turbulence. This limits the range for target recognition and identification [1,2].

The strength of atmospheric turbulence varies rapidly with time (Figure 1), so that there is a finite probability that a particular short-exposure snapshot will not suffer from significant loss of resolution. This fact can be exploited via the concept of “lucky frame selection” [3,4], in which multiple short-exposures are taken and analysed to determine the degree of atmospheric blurring. Those frames which suffer from an unacceptable amount of blurring are rejected, keeping only the “lucky” frames which have not been significantly degraded by the atmosphere. This technique permits high-resolution imagery to be obtained in conditions where a single long-exposure image would suffer from substantial loss of resolution.

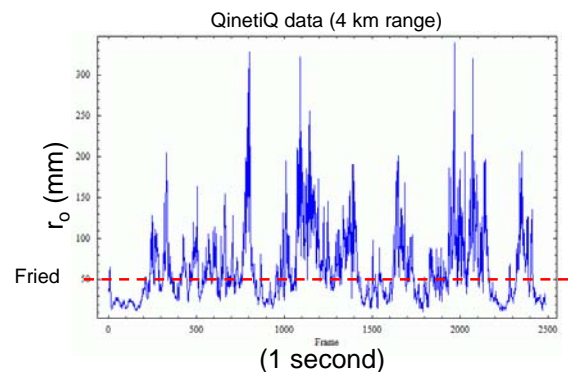


Figure 1: Variation of Fried parameter  $r_0$  over 1 second at intervals of 0.4ms. The high peaks correspond to instants where the atmospheric turbulence is weak and near diffraction-limited imagery may be obtained.

Fried [5] has calculated the probability of an individual frame being “lucky” as

$$P \approx 5.6 \exp \left[ -0.1577 \left( \frac{D}{r_0} \right)^2 \right] \quad (1)$$

which is valid for  $D/r_0 > 3.5$ .  $D$  is the aperture diameter and  $r_0$  is the Fried parameter. For smaller values of  $D/r_0$  the turbulence only induces image jitter without

any blurring, and consequently every frame is “lucky”. This is shown in Figure 2.

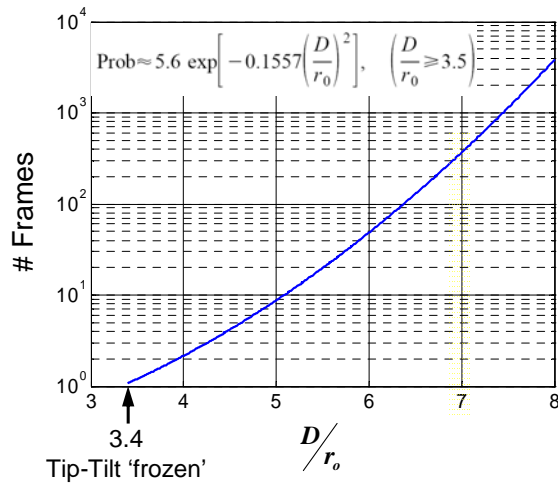


Figure 2: Average number of frames required to obtain one “lucky” frame, as a function of  $D/r_0$ .

Fried’s formula is valid for an imaging system with a spatially invariant point spread function (PSF), i.e. when the field of view (FOV) is sufficiently small that the atmospheric turbulence is constant across the FOV. For typical terrestrial imaging applications the atmospherically induced aberrations vary across the FOV of the imager, becoming decorrelated over a relatively small angle known as the isoplanatic angle,  $\theta_0$ , typically 10’s of  $\mu\text{rad}$ . In these circumstances, the image quality will vary across the FOV, with some regions having high resolution and others suffering from atmospheric blurring. The image may be regarded as a set of  $N$  ( $N \sim (FOV/\theta_0)^2$ ) independent sub-images, each with a probability  $P$  of being lucky according to the Fried formula. It is clear that the probability of the entire FOV being lucky is  $P_{FOV} = P^N$ , i.e. the probability of an entire “lucky frame” diminishes rapidly with increasing FOV.

To overcome this limitation the technique of “lucky sub-frame selection” may be employed, in which the image is analysed to determine which, if any, regions within the FOV are of high quality. Instead of a single image quality measurement for the entire frame, an image quality map is

generated, and rather than keeping or rejecting an entire frame, the high quality regions of every frame are kept and the low quality regions rejected. The image fragments from multiple frames are then assembled into a composite high quality image.

A typical approach to lucky sub-frame selection is to read out the entire high-resolution image, divide it into segments, and calculate the image sharpness for each segment. Each segment is then either retained or rejected according to whether the sharpness exceeds a preset threshold.

Since a single high quality composite image requires many raw frames from the imager to construct, it is desirable to operate such a system at high frame rate in order to update the composite image at a reasonable rate. It is therefore advantageous to have a simple and rapid method for estimating the image quality across the FOV. This paper describes an initial investigation into the use of low-resolution phase-diverse images to provide the image quality metric.

### An Image Quality Metric based on phase-diversity

The principle of using phase-diverse images for lucky sub-frame selection is based on the fact that the point-spread-function (PSF) of a defocused imaging system is invariant to the sign of the defocus if, and only if, the incoming wavefront at the system pupil is aberration-free.

The concept is thus to form two images of the scene with equal and opposite amounts of defocus. Those regions of the scene which are imaged with little or no atmospheric degradation will have the same PSF in both the phase-diverse images, and thus the two images will be near-identical in those regions. Conversely, those regions of the scene which are imaged with significant aberrations from atmospheric turbulence will have different PSFs in the

two phase-diverse images and the two images will be different in those regions. This is shown in Figure 3.



Figure 3a: In focus and phase diverse point spread functions for no aberration. The phase diverse PSFs are identical.



Figure 3b: In focus and phase diverse point spread functions with 1 wave of astigmatism. The phase diverse PSFs are different.

In order to select lucky sub-frames it is necessary to compare the two images on a pixel-by-pixel basis, so that a pair of phase-diversity images of  $M \times M$  pixels provides  $M^2$  individual metrics, each one measuring the image quality in the corresponding area within the FOV. The metric is thus simply comparing two values,  $I_1$  and  $I_2$  (the intensity in the specified pixel in each phase-diverse image).

The metric used is the absolute normalised difference between the pixels,

$$m = \left| \frac{I_1 - I_2}{I_1 + I_2} \right| \quad (2)$$

This calculation requires only 4 mathematical operations (subtraction, addition, division and absolute value), so the computational effort is small compared to the equivalent image sharpness calculation (as discussed in the section “Speed of operation”).

The absolute normalised difference varies between 0 and 1, with low values indicating

high image quality and high values indicating low image quality. The metric is invariant with respect to a scaling of the intensities, i.e. it is not affected by the overall intensity of the image at that point. This is important if the metric is to be equally valid for both bright and dark regions of the image. In particular, if the lucky sub-framing concept were to be used with an active imaging system such as BIL, the presence of rapidly varying scintillation on the scene from atmospheric degradation of the illuminator beam would cause a fluctuating intensity distribution from frame to frame. In this context the normalisation of the image quality metric is crucial, or the system would be biased towards selecting regions of the FOV which were not illuminated. A schematic showing the principle of lucky sub-frame selection using low-resolution phase-diverse images is shown in Figure 4.

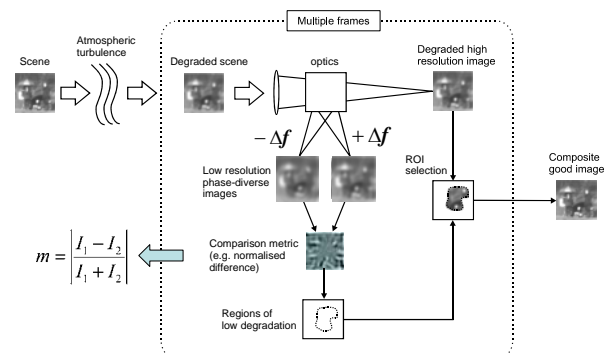


Figure 4: Comparison of two low-resolution phase-diverse (defocused) images enables identification of regions of high-quality in the FOV.

## Modelling

A simple model of the system has been written in *Mathematica* in order to prove the concept and permit an initial performance analysis of lucky sub-frame selection using phase-diverse images. This model uses just a single mode of atmospheric wavefront aberration, defocus, which permits the same PSF to be applied to multiple points in the scene. A model using a complete set of aberration modes would require a separate PSF to be calculated for each pixel, greatly increasing the model run time.

The model starts with a  $128 \times 128$  pixel image representing the unaberrated scene, and a  $128 \times 128$  aberration map that gives the degree of atmospheric defocus for each pixel in the scene. The aberration map is digitised to a small number of discrete levels, as this reduces the number of point spread functions that must be calculated from  $128^2=16384$  to perhaps 20, greatly speeding up the code. Three images are calculated from this data; the high-resolution  $128 \times 128$  image, and two  $32 \times 32$  phase-diverse (defocused) images. The phase-diverse images are then compared using the normalised intensity difference metric to identify those regions which are substantially the same in both images, and the corresponding regions of the high resolution image are extracted and sent to the frame composition algorithm.

A typical single-frame run of the model is shown in Figure 5, in which, for clarity, only five different defocus levels are in the aberration map.

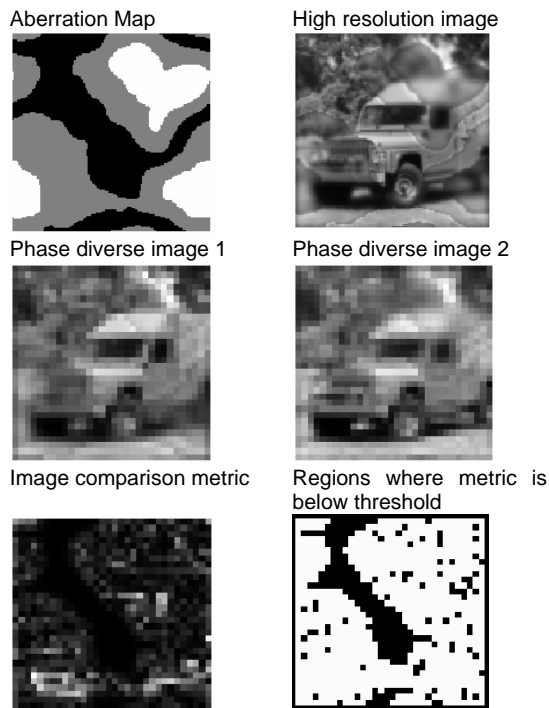


Figure 5: Typical single-frame run of the proof-of-concept model. The unaberrated regions of the scene correspond to the black areas in the aberration map. The black areas in the thresholded metric are the areas determined to be of high image quality.

The proof-of-concept model was run for both a random scene (i.e. a  $128 \times 128$  array of random numbers) and for a scene consisting of a picture of a jeep. The model looped through 100 random realisations of the aberration map. The model outputs two images, one being simply the sum of all the degraded images (the long exposure image) and the other being the composite image from the sub-frame selections. The ratio of the contrast in the two images was plotted as a function of spatial frequency to compare the two. The results are shown in Figure 6.

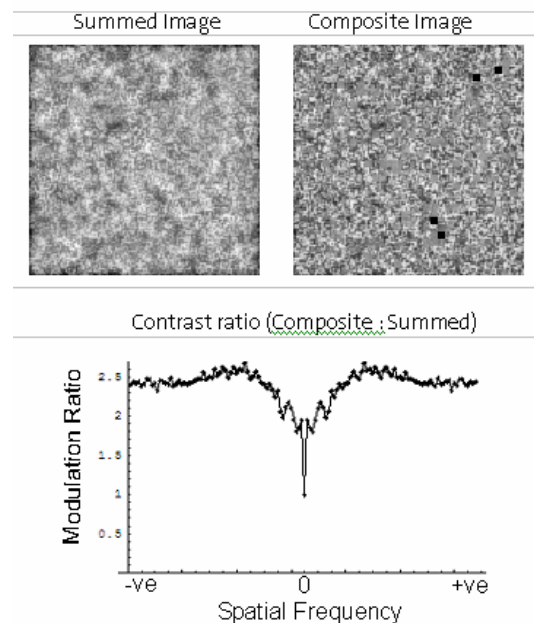


Figure 6: A composite image assembled from the high-quality regions in 100 short exposures has better resolution than the long exposure (summed) image. The modulation of high spatial frequencies is improved by a factor of 2 – 2.5.

### Speed of operation

One of the principal advantages of the phase-diversity approach to sub-frame selection is a reduction in the calculation time relative to more traditional image sharpness calculations. Referring to Figure 7, a simple comparison of the two approaches may be obtained as follows. Consider a high resolution image of  $N \times N$  pixels, with associated low resolution phase-diverse images of  $M \times M$  pixels. The sub-frame cell size in the high resolution image is defined by the area covered by a

single pixel in the low resolution phase-diverse images. Thus the total number of pixels in a sub-frame cell is  $(N/M)^2$ . The standard formula for image sharpness is given by [6]

$$S = \frac{\sum_j (I_j^2)}{(\sum_j I_j)^2} \quad (3)$$

where the sum is over all pixels in the image or sub-frame. For a total of  $(N/M)^2$  pixels, the number of basic operations (additions, multiplications, subtractions and divisions) in computing the sub-frame sharpness is  $3(N/M)^2+2$ . The calculation for a single sub-frame cell using the phase-diversity approach involves computing only the normalised difference between two pixels, as defined by Equation 2, i.e. a total of 4 operations. There are  $M^2$  sub-frame cells in the whole image, thus the total computational effort in analysing the entire FOV is given by

Image sharpness :  $3N^2 + 2M^2$  operations

Phase diversity :  $4M^2$  operations

For example, in the proof-of-concept model developed in this study,  $N=128$  and  $M=32$ . The number of basic operations is therefore:

Image sharpness : 51200 operations

Phase diversity : 4096 operations

The phase-diversity approach involves fewer operations by a factor of 13, offering a substantial reduction in the calculation time over the image sharpness method. This reduced calculation time will be important in a high frame-rate system attempting to deliver real-time imagery.

In the limit of  $N \gg M$ , the ratio of the calculation time for the phase-diversity approach to the sharpness calculation tends towards

$$R = \frac{3}{4} \left( \frac{N}{M} \right)^2$$

The computational effort involved in assembling the multiple sub-frames into a single composite frame is neglected in this analysis, since this is common to both approaches.

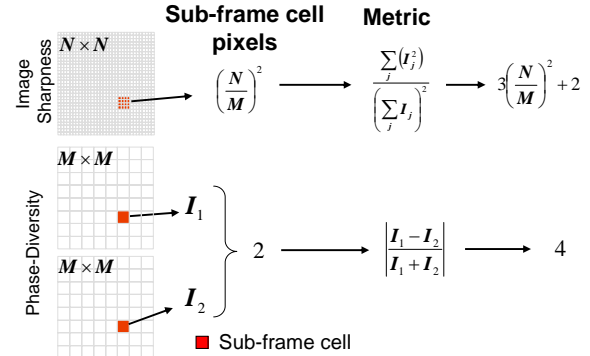


Figure 7: Comparison of the calculations required for sub-frame selection using image sharpness and phase-diversity.

A further improvement in speed is envisaged for imaging systems using a CMOS sensor chip with random access readout. In such a system it may be possible to read out only those pixels of the high-resolution image which are in regions of high quality, rather than reading out the entire high-resolution image and subsequently selecting the high quality regions. This would reduce the amount of data being read out of the chip and thereby allow an increase in frame-rate.

### Practical implementation

In order for the normalised intensity difference to have a null in regions of the image with little or no atmospheric aberration, the phase diverse images must be formed with equal and opposite amounts of defocus. Additionally, due to the rapid fluctuations in the atmospheric turbulence, the images must be obtained simultaneously. This requires either accurate synchronisation between two cameras or that both images are formed on a single detector.

Phase-diverse images satisfying these conditions can be obtained, for narrow-band imaging, by the use of an Image Multiplex (IMP<sup>®</sup>) grating [7]. The grating provides

both a beam-splitting and a defocusing effect, forming images in the +1 and -1 diffraction orders which are spatially separated on the sensor and which have equal and opposite amounts of defocus. The image formed in the 0<sup>th</sup> diffraction order is on-axis and has no defocus. This order may be suppressed if desired, by the use of a grating with a half-wave phase step. The use of an IMP<sup>®</sup> grating for generating the phase-diverse images is illustrated in Figure 8.

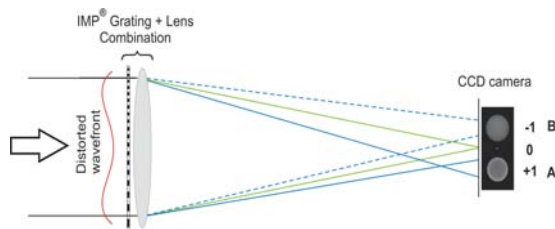


Figure 8: An IMP<sup>®</sup> grating in conjunction with a focussing lens provides defocused images in the  $\pm 1$  diffraction orders, either side of the focussed image in the 0 order.

One possible implementation would form both the high-resolution image and the two phase-diverse images on the same detector, using pixel binning to reduce the resolution of the phase-diverse images. This approach may be particularly suitable for imaging systems with expensive sensor arrays, where it is desirable not to require an additional sensor for the phase-diversity images.

The IMP<sup>®</sup> grating approach is not suitable for broadband imaging because of angular dispersion. That is, the angular separation of the diffraction orders is proportional to wavelength, leading to chromatic smearing of the phase-diverse images. Since the smearing occurs in opposite directions in the two images, the normalised intensity difference will no longer be zero in the absence of atmospheric aberrations.

Thus, for broadband imaging it will be necessary to identify an alternative scheme for forming the phase-diverse images without dispersion, whilst preferably

retaining the single-sensor advantage of the IMP<sup>®</sup> grating scheme.

### Future Work

One feature of atmospherically degraded imagery which has not been considered in detail in this study is image distortion. Image distortion arises from anisoplanatic tip/tilt, i.e. image jitter which varies across the FOV. Distortion changes the shape of objects in the scene but does not cause any blurring, and therefore it is not identified as degradation by the normalised difference metric. This has implications for the image composition algorithm, since each high-resolution image fragment will be displaced in the image plane by some unknown amount and direction. Future work on the phase-diversity sub-frame selection concept will have to address this issue to identify ways of correctly stitching together the image fragments to remove the distortion.

Note that the problem of image distortion is also present when using an image sharpness metric rather than phase-diversity, because image sharpness is unaffected by distortion. The simple and fast model used in this study was sufficient to prove the validity of the phase-diversity approach to lucky sub-frame selection. However, further investigation of the concept will require a substantial amount of realistic data, incorporating the full atmospheric wavefront (rather than just defocus), image distortion, correct spatio-temporal statistics (rather than a series of perfectly uncorrelated snapshots), sensor characteristics, chromatic effects such as dispersion and scene spectral content, non-atmospheric aberrations in the imaging system and three-dimensional scenes. The modelling required to incorporate these effects is highly complex and time consuming, and would inevitably include approximations (such as modelling the three-dimensional turbulence distribution as a single two-dimensional phase screen) and assumptions.

We propose that a programme of future work on this concept should include the construction of a phase-diversity imager to take real imagery in the field. Such a system would allow us to obtain large amounts of data with which to investigate the method in more detail.

### Conclusions

The precursor programme found that phase diversity provides a computationally efficient method for discriminating regions of good quality within an atmospherically degraded image. The proof-of-concept model shows an improvement by a factor of ~2.5 in the modulation transfer function (Figure 6). The key advantage of the phase diversity approach over the image sharpness calculation is an increase in speed.

The phase-diversity calculation is faster than the traditional image sharpness calculation by a factor of at least 13, assuming at least 4x4 pixels are required to determine an image sharpness metric compared to 2 pixels (one for each phase diversity image) for the wavefront sensor metric. This refers only to the calculation time once the data has been read from the sensor. The phase diversity approach also saves time by only reading out two low-resolution images prior to the calculation, rather than reading the entire frame as is required by the image sharpness method.

Additionally, if the high-resolution image were recorded on a random access sensor, then only the low degradation regions would need to be read out, thereby allowing increased frame rates and consequently a reduction in the time needed to form the high-resolution composite image.

### References

1. M. C. Roggemann and B. M. Welsh, *Imaging through Turbulence*, CRC Press, Boca Raton, FL (1996).

2. Carrano, C. J. "Speckle imaging over horizontal paths." In: Gonglewski, J. D., Vorontsov, M. A., Gruneisen, M. T., Restaino, S. R. (ed.). *High-Resolution Wavefront Control: Methods, Devices and Applications IV*, SPIE Vol. 4825 (2002), 109-120.
3. M. C. Roggemann, C. A. Stoudt, and B. M. Welsh, "Image spectrum signal-to-noise ratio improvements by statistical frame selection for adaptive optics imaging through atmospheric turbulence," *Opt. Eng.* 33, 3254–3264 (1994).
4. Ford, S. D., Roggemann, M. C., Welsh, B. M. "Frame selection performance limits for statistical image reconstruction of adaptive optics compensated images." *Optical Engineering*. 1996, 35(4), 1025-1034
5. Fried, D. L. "Probability of getting a lucky short-exposure image through turbulence." *J. Opt. Soc. Am.* 1978, 68, 1651-1658.
6. R. A. Muller and A. Buffington, "Real-time correction of atmospherically degraded telescope images through image sharpening," *J. Opt. Soc. Amer.*, vol. 64, no. 9, pp. 1200–1210, 1974.
7. Blanchard, P. M., Greenaway, A. H. "Simultaneous multi-plane imaging with a distorted diffraction grating." *Appl. Opt.* 1999, 38(32), 6692-6699.

### Acknowledgements

The work reported in this paper was funded by the Electro-Magnetic Remote Sensing (EMRS) Defence Technology Centre, established by the UK Ministry of Defence and run by a consortium SELEX Sensors and Airborne Systems, Thales Defence, Roke Manor Research and Filtronic.